Letter

Synthesis of Uniform Hollow Oxide Nanoparticles through Nanoscale Acid Etching

Kwangjin An, Soon Gu Kwon, Mihyun Park, Hyon Bin Na, Sung-Il Baik, Jung Ho Yu, Dokyoon Kim, Jae Sung Son, Young Woon Kim, In Chan Song, Woo Kyung Moon, Hyun Min Park, and Taeghwan Hyeon

Nano Lett., **2008**, 8 (12), 4252-4258 • Publication Date (Web): 14 November 2008

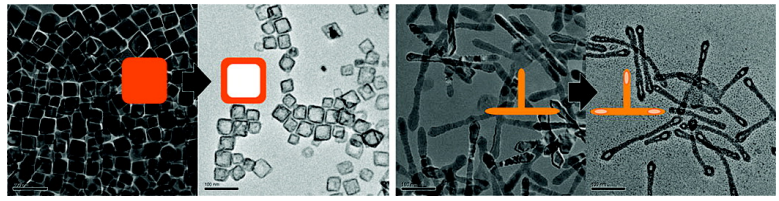

NANO LETTERS

2008
Vol. 8, No. 12
4252-4258

Synthesis of Uniform Hollow Oxide Nanoparticles through Nanoscale Acid Etching

Kwangjin An,[†] Soon Gu Kwon,[†] Mihyun Park,[†] Hyon Bin Na,[†] Sung-Il Baik,[‡] Jung Ho Yu,[†] Dokyoon Kim,[†] Jae Sung Son,[†] Young Woon Kim,[‡] In Chan Song,[§] Woo Kyung Moon,[§] Hyun Min Park,[||] and Taeghwan Hyeon*[,†]

National Creative Research Initiative Center for Oxide Nanocrystalline Materials, School of Chemical and Biological Engineering, School of Materials Science and Engineering, Seoul National University, Seoul 151-744, Korea, Diagnostic Radiology, Seoul National University Hospital, the Institute of Radiation Medicine, Medical Research Center, Seoul National University, Seoul 110-744, Korea, and New Material Evaluation Center, Korea Research Institute of Standards and Science, Taejon 305-600, Korea

Received July 2, 2008; Revised Manuscript Received September 20, 2008

ABSTRACT

We synthesized various hollow oxide nanoparticles from as-prepared MnO and iron oxide nanocrystals. Heating metal oxide nanocrystals dispersed in technical grade trioctylphosphine oxide (TOPO) at 300 °C for hours yielded hollow nanoparticles retaining the size and shape uniformity of the original nanocrystals. The method was highly reproducible and could be generalized to synthesize hollow oxide nanoparticles of various sizes, shapes, and compositions. Control experiments revealed that the impurities in technical grade TOPO, especially alkylphosphonic acid, were responsible for the etching of metal oxide nanocrystals to the hollow structures. Elemental mapping analysis revealed that the inward diffusion of phosphorus and the outward diffusion of metal took place in the intermediate stages during the etching process. The elemental analysis using XPS, EELS, and EDX showed that the hollow nanoparticles were amorphous metal oxides containing significant amount of phosphorus. The hollow nanoparticles synthesized from MnO and iron oxide nanocrystals were paramagnetic at room temperature and when dispersed in water showed spin relaxation enhancement effect for magnetic resonance imaging (MRI). Because of their morphology and magnetic property, the hollow nanoparticles would be utilized for multifunctional biomedical applications such as the drug delivery vehicles and the MRI contrast agents.

Hollow nanoparticles have attracted much interest from researchers in various disciplines for their many technological applications including drug delivery. Recently, various hollow nanoparticles of oxides and chalcogenides have been synthesized through a nanoscale Kirkendall effect resulting from different interdiffusion rates of two materials.[1] Iron oxide nanoparticles have been applied to various biomedical applications including magnetic resonance imaging (MRI) contrast agents, magnetically guided drug delivery vehicles, and the magnetic separation of biological materials.[2] Several kinds of hollow iron oxide nanoparticles have been recently synthesized.[3] For example, hollow magnetite nanocapsules fabricated by a wrap-bake-peel process by the present group and used as a drug delivery vehicle as well as a T_2 MRI contrast agent.[3a] Recently, a new T_1 MRI contrast agent was developed using MnO nanoparticles.[4] This letter presents a novel method for the synthesis of uniform hollow oxide nanoparticles via a controlled nanoscale etching of metal oxide nanocrystals in the presence of trioctylphosphine oxide (TOPO) and alkylphosphonic acid. This nanoscale etching process is very simple and generally applicable to iron oxide and MnO nanocrystals with different sizes, shapes, and compositions. Interestingly, the hollow nanoparticles obtained retained their original size and contour before etching. When dispersed in water, they showed the T_1 and T_2 relaxation enhancement effect in MRI.

For the synthesis of hollow nanoparticles, the as-prepared metal oxide nanocrystals were redispersed in technical grade TOPO and heated at 300 °C for hours under inert atmosphere. During heating, the dispersion became colorless and trans-

* To whom correspondence should be addressed. E-mail: thyeon@snu.ac.kr.
[†] National Creative Research Initiative Center for Oxide Nanocrystalline Materials, School of Chemical and Biological Engineering, Seoul National University.
[‡] School of Materials Science and Engineering, Seoul National University.
[§] Diagnostic Radiology, Seoul National University Hospital, and the Institute of Radiation Medicine, Medical Research Center, Seoul National University.
[||] Korea Research Institute of Standards and Science.

10.1021/nl8019467 CCC: $40.75
Published on Web 11/14/2008

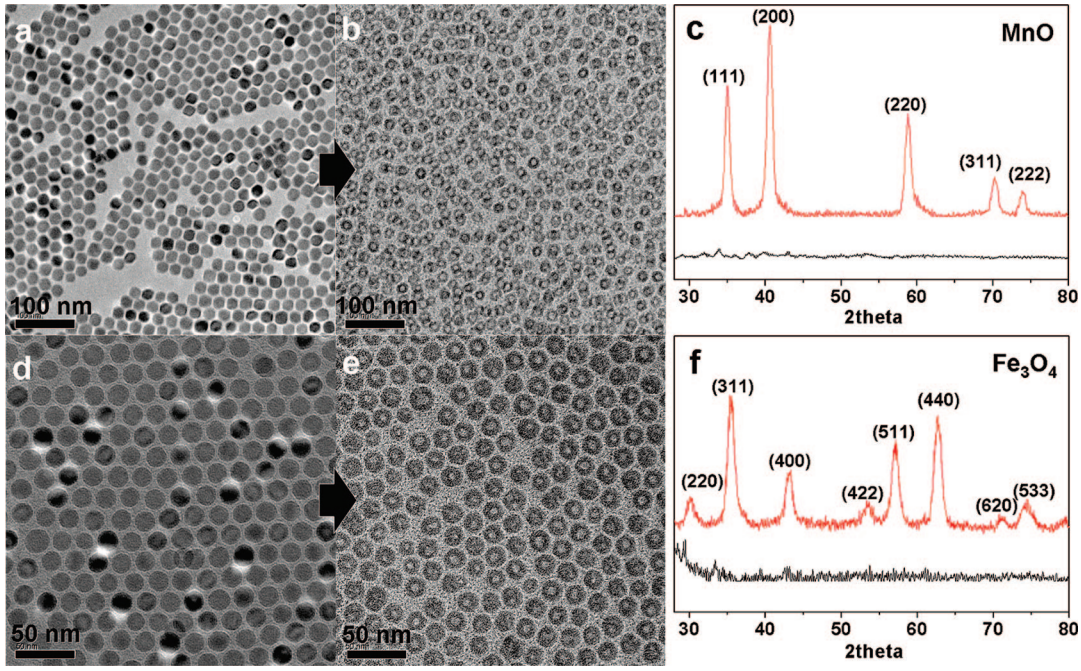

Figure 1. TEM images showing the changes from solid nanocrystals of 18 nm-sized MnO (a) and 20 nm-sized Fe_3O_4 nanocrystals (d) to the corresponding hollow oxide nanoparticles (b,e) through the etching process. The corresponding XRD patterns before (red) and after (black) the etching process are shown for MnO (c) and iron oxide (f), respectively.

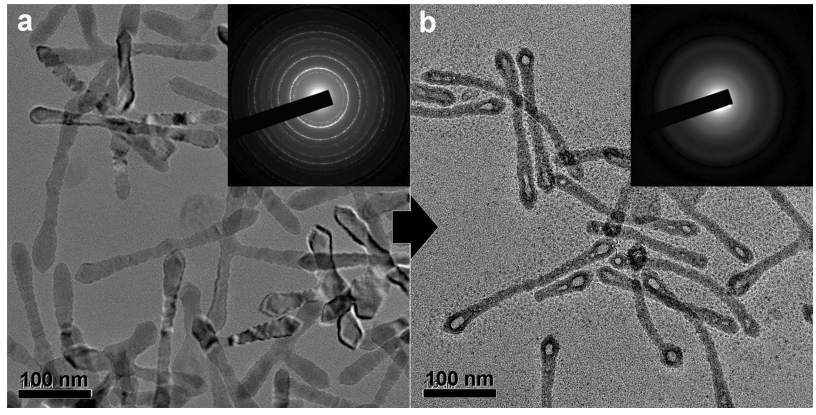

Figure 2. TEM images of dumbbell-shaped solid MnO nanocrystals (a) and the corresponding hollow oxide nanoparticles after the etching process (b). In the insets, the corresponding ED patterns are shown.

parent regardless of the nature of metal oxide nanocrystals dispersed. After cooling to room temperature, nanoparticles were precipitated as white powder with excess acetone and methanol (for experimental details, see Supporting Information). This process was applied to MnO and iron oxide nanocrystals.[5] Figure 1 shows transmission electron microscopy (TEM) images of hollow nanoparticles synthesized from cuboctahedral MnO and spherical Fe_3O_4 nanocrystals. As shown in the figure, the high uniformity of the original metal oxide nanocrystals was retained through the etching process.[6] The same etching process was generally applicable to a wide range of sizes, namely, from 11 to 24 nm for both MnO and Fe_3O_4 nanocrystals (see Figure S1 in Supporting Information). Interestingly, hollow nanostructures were also obtained from dumbbell-shaped MnO nanocrystals[7] (Figure 2), which have a more complicated morphology compared to those in Figure 1, through the same etching process. Moreover, using metal oxide nanocrystals of different compositions including cubic α-Fe_2O_3 (Figure 3) and manganese ferrite (see Figure S2 in Supporting Information) as the starting materials were successful for the synthesis of hollow nanoparticles. Consequently, the current method for the synthesis of hollow nanoparticles is widely applicable for various sized, shapes, and compositions of metal oxide nanocrystals. The size and the shape were controlled by simply using different metal oxide nanocrystals as the starting materials. The whole process was simple and highly reproducible.

Characterization of hollow nanocrystals synthesized from different metal oxide nanocrystals revealed that they shared some common features: The minimum wall thickness observed was always around 3 nm for all hollow nanoparticles. The size and the shape of the original metal oxide nanocrystals were unchanged through the etching process (for the comparison of the size distribution of the nanoparticles before and after the etching process, see Figure S3 in

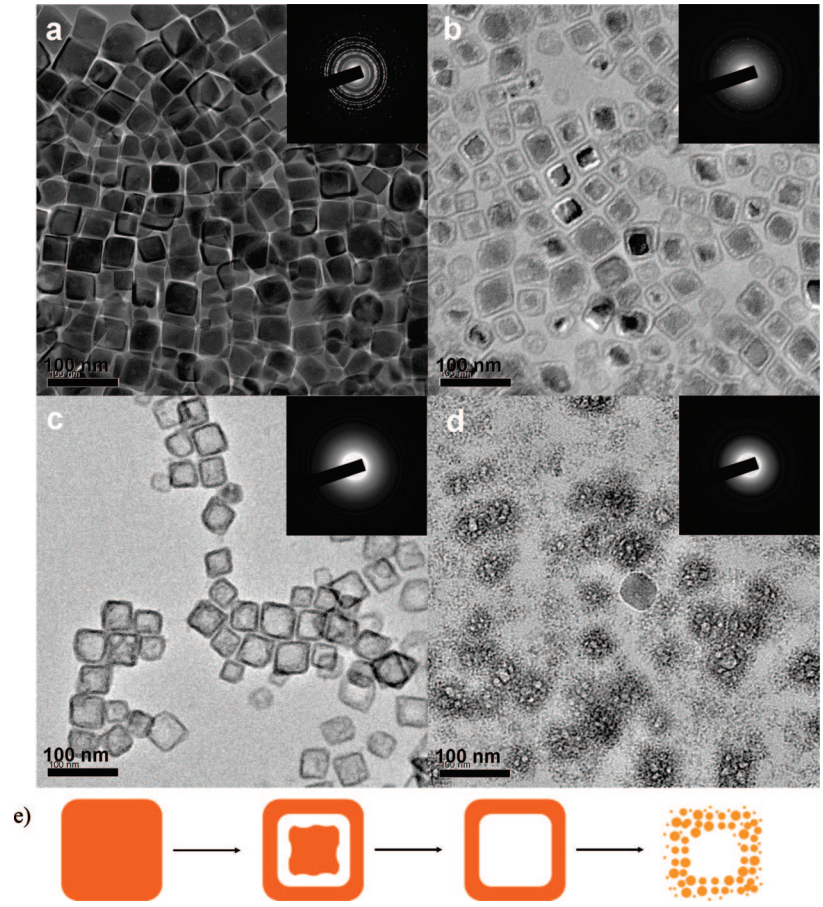

Figure 3. TEM images showing the stages of the etching process for α-Fe_2O_3 nanocubes: solid α-Fe_2O_3 nanocubes before the etching (a), core−shell-void intermediates (b), hollow nanoboxes (c), and fragmented particles (d). In the insets, the corresponding electron diffraction patterns are shown. (e) A schematic for the evolution of the morphologies of the particles shown in panels a−d.

Supporting Information). On the other hand, when metal oxide nanocrystals smaller than 10 nm were etched, they dissolved without retaining the original size and shape. According to X-ray diffraction (XRD) and electron diffraction (ED) data shown in Figures 1−4, hollow nanoparticles were amorphous regardless of the starting materials.[8] According to X-ray photoelectron spectroscopy (XPS) data, they contained metal cations from the starting metal oxide nanocrystals. As shown in Figure 5, there was no significant change in the oxidation state of metal cations before and after the etching process. Notably, the magnetic property of MnO nanocrystals was almost identical before and after the etching process whereas the magnetization behavior of Fe_3O_4 nanocrystals was changed greatly from superparamagnetic to paramagnetic (Figure 6). It is known that MnO nanocrystals are weakly ferromagnetic at low temperature even though bulk MnO is antiferromagnetic.[9] The magnetic moment of MnO nanocrystals comes from Mn^{2+} ions at the partially amorphous surface with high surface energy. On the other hand, Fe_3O_4 nanocrystals are ferrimagnetic and the magnetic moment of Fe^{2+}/Fe^{3+} ions are stabilized by the crystal symmetry. As a result, the magnetic property of amorphous hollow nanoparticles containing Mn^{2+} ions would be similar to that of MnO nanocrystals while Fe-containing hollow nanoparticles were far different from Fe_3O_4 nanocrystals in their magnetic properties. The elemental analysis

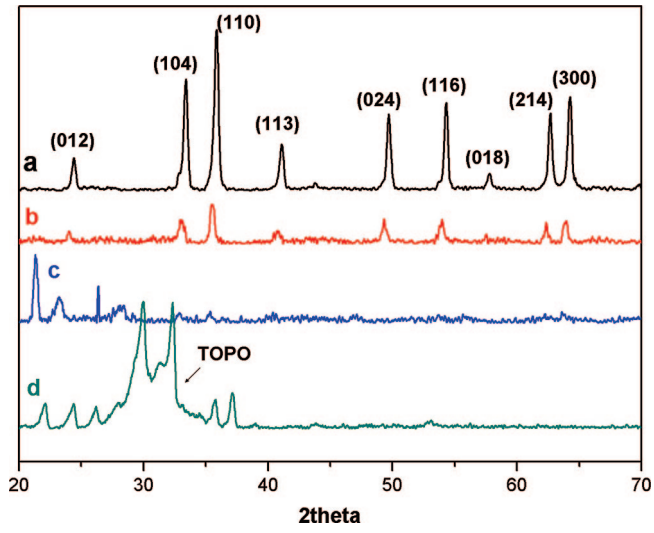

Figure 4. XRD patterns for the corresponding stages during the etching process shown in Figure 3: solid α-Fe_2O_3 nanocubes (a), core−shell-void intermediates (b), hollow nanoboxes (c), and fragmented particles (d). The peaks from unwashed TOPO are indicated with an arrow.

revealed that hollow nanoparticles were composed of metal, phosphorus, and oxygen (see Figure S4 in Supporting Information). We believe that the current hollow oxide nanoparticles are of certain amorphous metal phosphate.

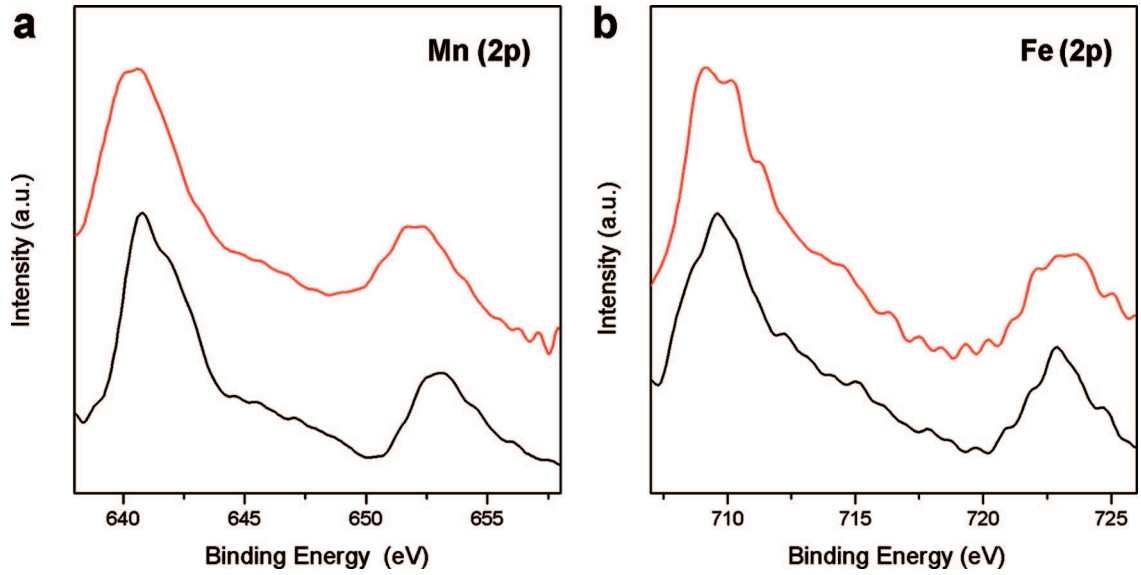

Figure 5. XPS spectra for MnO (a) and Fe_3O_4 (b) nanocrystals before (red) and after (black) the etching process.

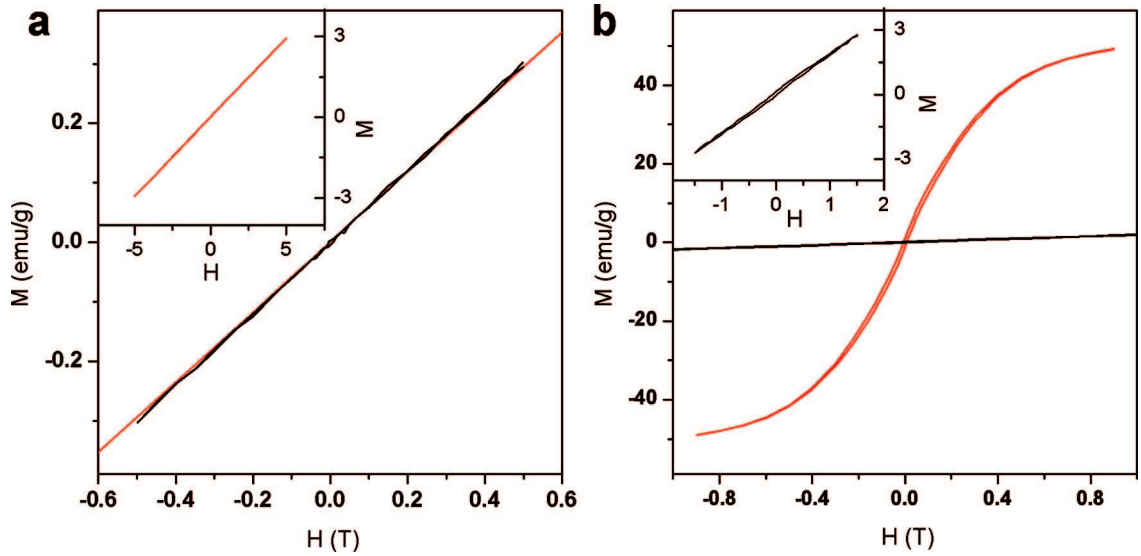

Figure 6. Magnetization curves for MnO (a) and Fe_3O_4 (b) nanocrystals before (red) and after (black) the etching process. The data were acquired at 300 K. The insets of panels a and b show the full-scale magnetization curves of MnO nanocrystals before the etching process and the Fe_3O_4 nanocrystals after the etching, respectively.

However, at this point of time the compositional and structural characterizations of these materials are not completed yet.

The synthetic chemistry of the current etching process was investigated by conducting a series of controlled experiments. At first, when highly pure (99%) TOPO was used for the etching process instead of the technical grade, no hollow nanoparticles were generated. It was reported that commercially available TOPO contains various impurities including alkylphosphine oxides, alkylphosphinates, alkylphosphonic acids, and alkylphosphinic acids, some of which strongly influence the synthesis of the nanocrystals.[10] Generally, the strong interaction of the impurities in TOPO such as alkylphosphonic acids in the synthesis of nanocrystals comes from their strong binding ability to metal cations.[11] Therefore, in the second step, we tested the role of alkylphosphonic acid by using mixtures of highly pure TOPO and various alkylphosphonic acids for the etching of MnO nanocrystals (for experimental details, see Supporting Information). When methyl- and hexyl-phosphonic acids were mixed with fixed amounts of TOPO and MnO nanocrystals, the nanocrystals quickly dissolved away at the melting temperature of TOPO (55 °C). On the other hand, when the reaction mixture containing tetradecylphosphonic acid was heated at 250 °C for one hour, partial dissolution of the nanocrystals occurred (see Figure S5 in Supporting Information). It is well known that the binding ability of alkylphosphonic acid decreases as the alkyl group gets bulkier due to the steric effect. These control experimental results confirmed that alkylphosphonic acid is responsible for the etching of metal oxide nanocrystals. It seems that during the etching process, alkylphosphonic acids coordinate to the metal cations on the surface of the metal oxide nanocrystals and

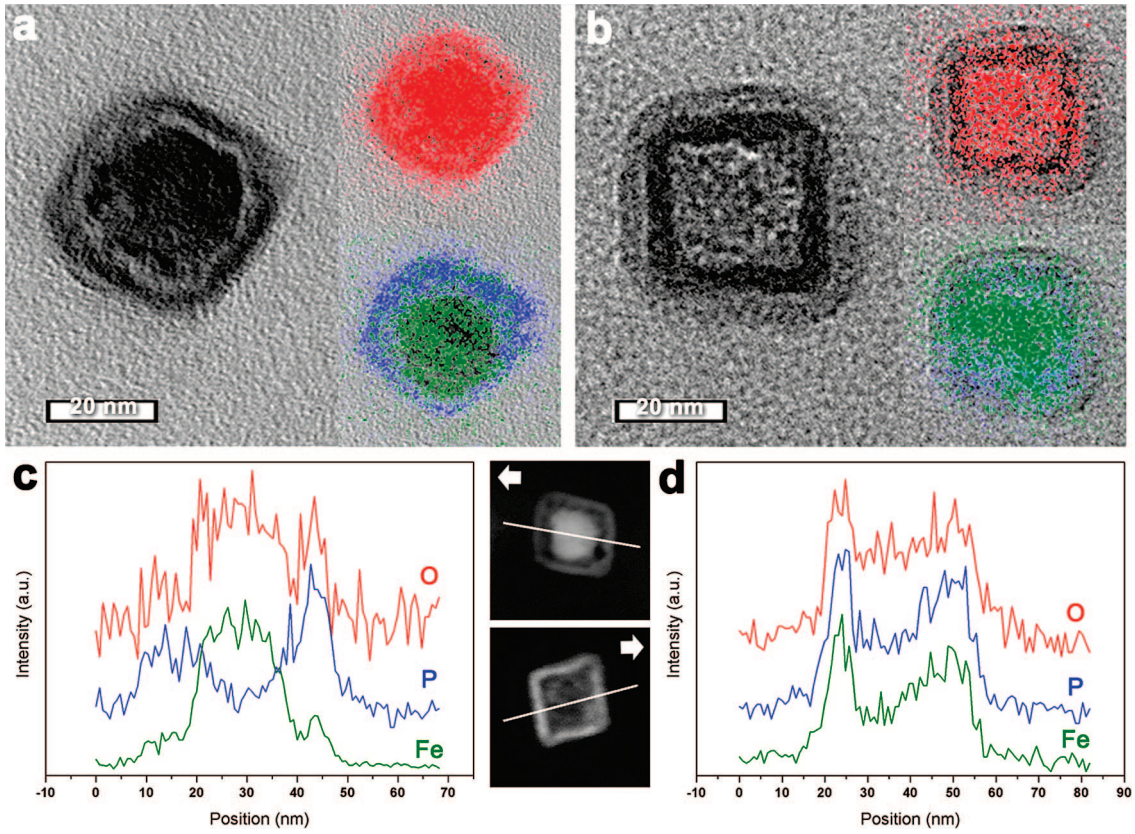

Figure 7. (a,b) High resolution TEM images of the core−shell-void intermediate (panel a) and the hollow nanoparticles (panel b). In the insets, the elemental mapping images for oxygen (red, upper) and iron and phosphorus (green and blue, lower) from EELS analysis are shown superimposed on the same TEM images in each panel. (c,d) The plots for the relative abundance of each element as functions of position for the core−shell-void intermediate (panel c) and the hollow nanoparticles (panel d) obtained by EDX line-scanning analysis.

form metal-phosphonate complexes, which dissolve into the solution.

To study the formation mechanism of hollow oxide nanoparticles, we chose the synthetic system using α-Fe_2O_3 nanocrystals as the starting materials because α-Fe_2O_3 nanocrystals were large enough (~50 nm) to observe the intermediates during the etching process.[12] As shown in Figure 3, there are four distinct stages in the course of the reaction: the initial solid metal oxide nanocrystals, the core−shell-void intermediate, the hollow structure, and, finally, the totally fragmented small-sized nanoparticles. The XRD data in Figure 4 indicate that the change from α-Fe_2O_3 phase to amorphous oxide phase was gradual and that these two phases coexisted in the core−shell-void intermediate.[1b] The similar processes have been reported in a number of previous reports on the synthesis of hollow nanostructures and were attributed to Kirkendall effect.[1] This effect comes from the diffusion of atoms or ions balanced with the counter-diffusion of vacancies in solid. For example, in a particulate morphology, the outward diffusion of the constituting materials and the simultaneous inward diffusion of vacancies result in the formation of void in the core. In the current system, it seems that the etching of metal cations by alkylphosphonic acid on the surface of metal oxide nanocrystals drives the outward diffusion of metal cations in the nanocrystals. Besides, as mentioned above, hollow nanoparticles contained phosphorus that seemed to have come from TOPO. TOP has been frequently used as phosphorus source for the synthesis of metal phosphide nanocrystals.[13] Given that phosphorus is supplied from the solution, there should be the inward diffusion of phosphorus via the surface of the nanocrystals. In summary, it seems that there are three diffusion processes during the formation of hollow nanoparticles: the outward diffusion of metal cations accompanied with the counter-diffusion of vacancies and the inward diffusion of phosphorus. We performed elemental mapping analysis of iron, phosphorus, and oxygen in the nanoparticles at the stages of the core−shell-void and the hollow structures to verify these three proposed diffusion processes (Figure 7). The elemental mapping images from electron energy loss spectroscopy (EELS) clearly show that the spatial distributions of the elements are quite different between these two stages. In the core−shell-void particle shown in Figure 7a, oxygen is nearly evenly distributed over the entire volume of the particle whereas phosphorus and iron exist dominantly in the shell and the core, respectively. Superimposing the elemental mapping images over the high resolution TEM image, it is evident that the void region dividing the shell and the core matches exactly with the boundary between the phosphorus and the iron regions, demonstrating that the shell is mainly composed of phosphorus oxide and the core is iron oxide. This result from EELS analysis is consistent with the data shown in Figure 7c obtained from energy dispersive X-ray spectroscopy (EDX) analysis. On the other hand, Figure 7b shows that, in a hollow particle, oxygen, phosphorus, and iron are equally distributed over the particle.

Scheme 1

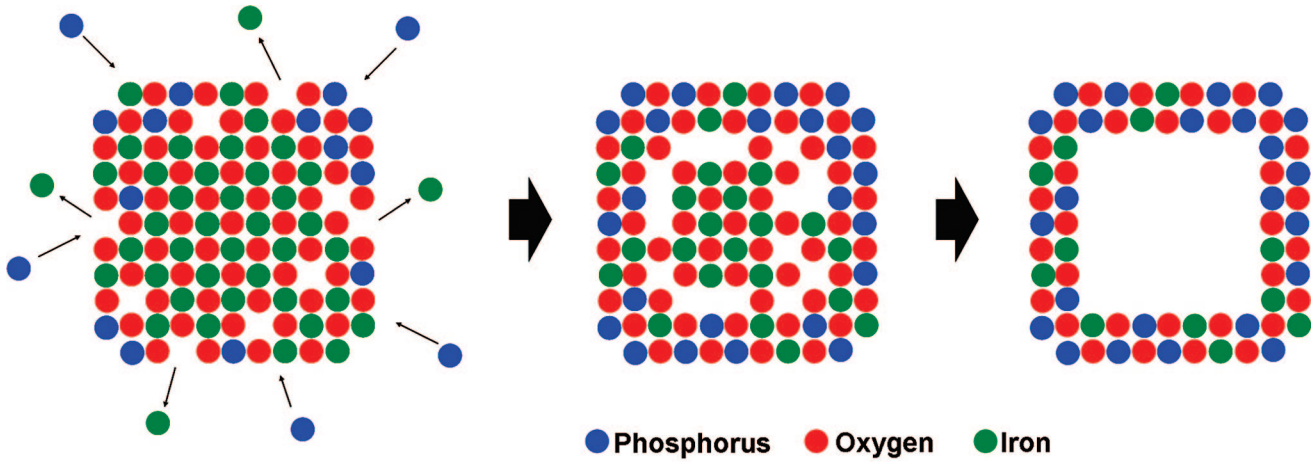

Table 1. Spin Relaxation Properties of the Solid Nanocrystals of MnO and Fe_3O_4 and the Corresponding Hollow Oxide Nanoparticles

relaxivity ($mM^{-1}s^{-1}$)	20 nm MnO	hollow (MnO)	11 nm Fe_3O_4	hollow (Fe_3O_4)
r_1	0.353	1.150	1.55	0.157
r_2	8.683	6.737	60.54	1.253

According to EDX data shown in Figure 7d, the relative ratio between these elements is kept constant at all positions, which means that the composition of the particle is homogeneous over the volume of the particle. The similar results were obtained from the same analysis of the nanoparticles of the intermediate stage in the synthetic system using MnO nanocrystals as the starting materials (see Figure S6 Supporting Information). On the basis of these observations, we devised a plausible mechanism for the formation of hollow oxide nanoparticles in the current synthetic system (Scheme 1). In the early stage of the etching process, metal cations dissolve into the solution by the coordination of alkylphosphonic acid, which increases the vacancy concentration near the surface of the particle. At the same time, phosphorus from the solution diffuses to the surface of the particle filling the vacancies. In the next stage, continued dissolution of metal cations and the supply of phosphorus transform the outer shell of the nanocrystal from metal oxide to phosphorus oxide. The outward diffusion of metal cations and the accumulation of vacancies inside the shell lead to the formation of the void between the core and the shell. Lastly, the diffusion of metal cations stops when the composition of the particle becomes homogeneous. Until the last stage, the shell composed of metal, phosphorus, and oxygen is maintained by the balance of the inward diffusion of phosphorus and the outward diffusion of metal.

To examine the applicability of hollow nanoparticles synthesized from MnO and Fe_3O_4 nanocrystals as the MRI contrast agents, the spin relaxation properties of the water-dispersed hollow nanoparticles were examined with a 1.5-T human clinical scanner, and the results are summarized in Table 1 (for detailed description for the water dispersibilization process, see Supporting Information). Hollow nanoparticles containing Mn^{2+} ions showed positively enhanced T_1 relaxation. The value of r_1 for these particles was larger than that of the MnO nanocrystals of the similar size, an effect presumably derived from the increased surface area of the hollow nanoparticles that enabled enhanced interaction between nanoparticles and water molecules. With that improved r_1 relaxivity, hollow nanoparticles from MnO nanocrystals can be used in the multifunctional nanomedical applications as the MRI contrast agent and the drug delivery vehicle, simultaneously. On the other hand, the r_2 relaxivity of 11 nm-sized hollow nanoparticles synthesized from Fe_3O_4 nanocrystals was very low due to their low susceptibility as shown in the magnetization data shown in Figure 6b.

In conclusion, we synthesized hollow oxide nanoparticles of various sizes, shapes, and compositions using MnO and iron oxide nanocrystals as the starting materials and the technical grade TOPO as both the solvent and the etchant. This method is very simple and highly reproducible. The hollow nanoparticles synthesized were amorphous and composed of oxygen, phosphorus, and metal. We found that alkylphosphonic acid impurity in technical grade TOPO is responsible for the etching process. The opposite diffusion of phosphorus and metal cations within metal oxide nanocrystals accompanied by Kirkendall effect was suggested as the possible formation mechanism of the hollow nanoparticles. These hollow nanoparticles were paramagnetic at room temperature. When dispersed in water, they showed spin relaxation enhancement effect. Because of the unique hollow structure and the spin relaxation enhancement, the hollow oxide nanoparticles have potential for multifunctional biomedical applications such as the drug delivery vehicles and the MRI contrast agents.

Acknowledgment. The present work was supported by the Korea Science and Engineering Foundation (KOSEF) through the National Creative Research Initiative Program.

Supporting Information Available: Experimental details, TEM, XPS, elemental mapping with EDX, and particle size distribution histograms of the metal oxide nanocrystals and hollow nanoparticles are included. This material is available free of charge via the Internet at http://pubs.acs.org.

References

(1) (a) Yin, Y.; Rioux, R.; Erdonmez, C. K.; Hughes, S.; Somorjai, G. A.; Alivisatos, A. P. *Science* **2004**, *304*, 711–714. (b) Peng, S.; Sun, S. *Angew. Chem., Int. Ed.* **2007**, *46*, 4155–4158. (c) Cabot, A.; Puntes, V. F.; Shevchenko, E.; Yin, Y.; Balcells, L.; Marcus, M. A.; Hughes, S. M.; Alivisatos, A. P. *J. Am. Chem. Soc.* **2007**, *129*, 10358–10360. (d) Fan, H. J.; Knez, M.; Scholz, R.; Nielsch, K.; Pippel, E.; Hesse, D.; Zacharias, M.; Gösele, U. *Nat. Mater.* **2006**, *5*, 627–631. (e) Fan, H. J.; Gösele, U.; Zacharias, M. *Small* **2007**, *3*, 1660–1671. (f) Fan, H. J.; Knez, M.; Scholz, R.; Hesse, D.; Nielsch, K.; Zacharias, M.; Gösele, U. *Nano Lett.* **2007**, *7*, 993–997. (g) Chiang, R.-K.; Chiang, R.-T. *Inorg. Chem.* **2007**, *46*, 369–371. (h) Gao, J.; Liang, G.; Zhang, B.; Kuang, Y.; Zhang, X.; Xu, B. *J. Am. Chem. Soc.* **2007**, *129*, 1428–1433. (i) Liang, W.; Wang, X.; Zhuang, Y.; Xu, B.; Kuang, S.; Li, Y. *J. Am. Chem. Soc.* **2008**, *130*, 2736–2737. (j) Gao, J.; Zhang, B.; Zhang, X.; Xu, B. *Angew. Chem., Int. Ed.* **2006**, *45*, 1220–1223. (k) Yin, Y.; Erdonmez, C. K.; Cabot, A.; Hughes, S.; Alivisatos, A. P. *Adv. Funct. Mater.* **2006**, *16*, 1389–1399. (l) Henkes, A. E.; Vasquez, Y.; Schaak, R. E. *J. Am. Chem. Soc.* **2007**, *129*, 1896–1897. (m) Wang, Y.; Cai, L.; Xia, Y. *Adv. Mater.* **2005**, *17*, 473–477 (n) Shevchenko, E. V.; Bodnarchuk, M. I.; Kovalenko, M. V.; Talapin, D. V.; Smith, R. K.; Aloni, S.; Heiss, W.; Alivisatos, A. P. *Adv. Mater.*, Early view (adma.200702994).

(2) (a) Lee, J.-H.; Huh, Y.-M.; Jun, Y.-w.; Seo, J.-w.; Jang, J.-t.; Song, H.-T.; Kim, S.; Cho, E.-J.; Yoon, H.-G.; Suh, J.-S.; Cheon, J. *Nat. Med.* **2007**, *13*, 95–99. (b) Jun, Y.-w.; Huh, Y.-M.; Choi, J.-s.; Lee, J.-H.; Song, H.-T.; Kim, S.; Yoon, S.; Kim, K.-S.; Shin, J.-S.; Sur, J.-S.; Cheon, J. *J. Am. Chem. Soc.* **2005**, *127*, 5732–5733. (c) Song, H.-T.; Choi, J.-s.; Huh, Y.-M.; Kim, S.; Jun, Y.-w.; Suh, J.-S.; Cheon, J. *J. Am. Chem. Soc.* **2005**, *127*, 9992–9993. (d) Huh, Y.-M.; Jun, Y.-w.; Song, H.-T.; Kim, S.; Choi, J.-s.; Lee, J.-H.; Yoon, S.; Kim, K.-S.; Shin, J.-S.; Suh, J.-S.; Cheon, J. *J. Am. Chem. Soc.* **2005**, *127*, 12387–12391. (e) Weissleder, R.; Kelly, K.; Sun, E. Y.; Shtatland, T.; Josephson, L. *Nat. Biotechnol.* **2005**, *23*, 1418–1423. (f) Bulte, J. W. M.; Kraitchman, D. L. *NMR Biomed.* **2004**, *17*, 484–499. (g) Bulte, J. W. M.; Zhang, S.-C.; van Gelderen, P.; Herynek, V.; Jordan, E. K.; Duncan, I. D.; Frank, J. A. *Proc. Natl. Acad. Sci. U.S.A.* **1999**, *96*, 15256–15261. (h) Gu, H.; Xu, K.; Xu, C.; Xu, B. *Chem. Commun.* **2006**, 941–949.

(3) (a) Piao, Y.; Kim, J.; Na, H. B.; Kim, D.; Baek, J. S; Ko, M. K.; Lee, J. H.; Shokouhimehr, M.; Hyeon, T. *Nat. Mater.* **2008**, *7*, 242–247. (b) Kim, D.; Park, J.; An, K.; Yang, N.-K.; Park, J.-G.; Hyeon, T. *J. Am. Chem. Soc.* **2007**, *129*, 5812–5813.

(4) Na, H. B.; Lee, J. H.; An, K.; Park, Y. I.; Park, M.; Lee, I. S.; Nam, D.-H.; Kim, S. T.; Kim, S.-H.; Kim, S.-W.; Lim, K.-H.; Kim, K.-S.; Kim, S.-O.; Hyeon, T. *Angew. Chem., Int. Ed.* **2007**, *46*, 5397–5401.

(5) Park, J.; An, K.; Hwang, Y.; Park, J.-G.; Noh, H.-J.; Kim, J.-Y.; Park, J.-H.; Hwang, N.-M.; Hyeon, T. *Nat. Mater.* **2004**, *3*, 891–895.

(6) (a) Zeng, H.; Cai, W.; Liu, P.; Xu, X.; Zhou, H.; Klingshirn, C.; Kalt, H. *ACS Nano* **2008**, *2*, 1661–1670. (b) Kuo, C.-H.; Huang, M. H. *J. Am. Chem. Soc.*, **2008**, *130*, 12815−12820. (c) Zhao, X.; Yu, J. *J. Cryst. Growth* **2007**, *306*, 366–372.

(7) (a) Zitoun, D.; Pinna, N.; Frolet, N.; Belin, C. *J. Am. Chem. Soc.* **2005**, *127*, 15034–15035. (b) Zhong, X.; Xie, R.; Sun, L.; Lieberwirth, I.; Knoll, W. *J. Phys. Chem. B* **2006**, *110*, 2–4.

(8) Latham, A. H.; Wilson, M. J.; Schiffer, P.; Williams, M. E. *J. Am. Chem. Soc.* **2006**, *128*, 12632–12633.

(9) (a) Kodama, R. H. *J. Magn. Magn. Mater.* **1999**, *200*, 359–372. (b) Seo, W. S.; Jo, H. H.; Lee, K.; Kim, B.; Oh, S. J.; Park, J. T. *Angew. Chem., Int. Ed.* **2004**, *43*, 1115–1117. (c) Lee, G. H.; Hur, S. H.; Jeong, J. W.; Choi, B. J.; Kim, S. H.; Ri, H.-C. *J. Am. Chem. Soc.* **2002**, *124*, 12094–12095. (d) Jeong, U.; Teng, X.; Wang, Y.; Yang, H.; Xia, Y. *Adv. Mater.* **2007**, *19*, 33–60.

(10) (a) Wang, F.; Tang, R.; Buhro, W. E. *Nano Lett.*, **2008**, *8*, 3521−3524. (b) Kopping, J. T.; Patten, T. E. *J. Am. Chem. Soc.* **2008**, *130*, 5689–5698.

(11) (a) Peng, X.; Manna, L.; Yang, W.; Wickham, E. S.; Kadavanich, A.; Alivisatos, A. P. *Nature* **2000**, *404*, 59–61. (b) Peng, X. *Chem.Eur. J.* **2002**, *8*, 334–339. (c) Peng, Z. A.; Peng, X. *J. Am. Chem. Soc.* **2001**, *123*, 1389–1395. (d) Peng, Z. A.; Peng, X. *J. Am. Chem. Soc.* **2002**, *124*, 3343–3353.

(12) Wang, S. B.; Min, Y. L.; Yu, S.-H. *J. Phys. Chem. C* **2007**, *111*, 3551–3554.

(13) (a) Park, J.; Koo, B.; Hwang, Y.; Bae, C.; An, K.; Park, J.-G.; Park, H. M.; Hyeon, T. *Angew. Chem., Int. Ed.* **2004**, *43*, 2282–2285. (b) Park, J.; Koo, B.; Yoon, K. Y.; Hwang, Y.; Kang, M.; Park, J.-G.; Hyeon, T. *J. Am. Chem. Soc.* **2005**, *127*, 8433–8440. (c) Perera, S. C.; Tsoi, G.; Wenger, L. E.; Brock, S. L. *J. Am. Chem. Soc.* **2003**, *125*, 13960–13961. (d) Stamm, K. L.; Gamo, J. C.; Liu, G. Y.; Brock, S. L. *J. Am. Chem. Soc.* **2003**, *125*, 4038–4039. (e) Qian, C.; Kim, F.; Ma, L.; Tsui, F.; Yang, P. D.; Liu, J. *J. Am. Chem. Soc.* **2004**, *126*, 1195–1198.

NL8019467